Electronic Supplementary Information (ESI)

Development of novel ruthenium(II)-arene complexes displaying potent anticancer effects in glioblastoma cells

Priyaranjan Kumar,[a] Indranil Mondal,[b] Ritu Kulshreshtha,[b] and Ashis K. Patra*[,a]

Author address: [a] Department of Chemistry, Indian Institute of Technology Kanpur, Kanpur 208016, Uttar Pradesh, India

[b] Department of Biochemical Engineering and Biotechnology, Indian Institute of Technology Delhi, Hauz Khas, New Delhi 110 016, India

Supporting information contents

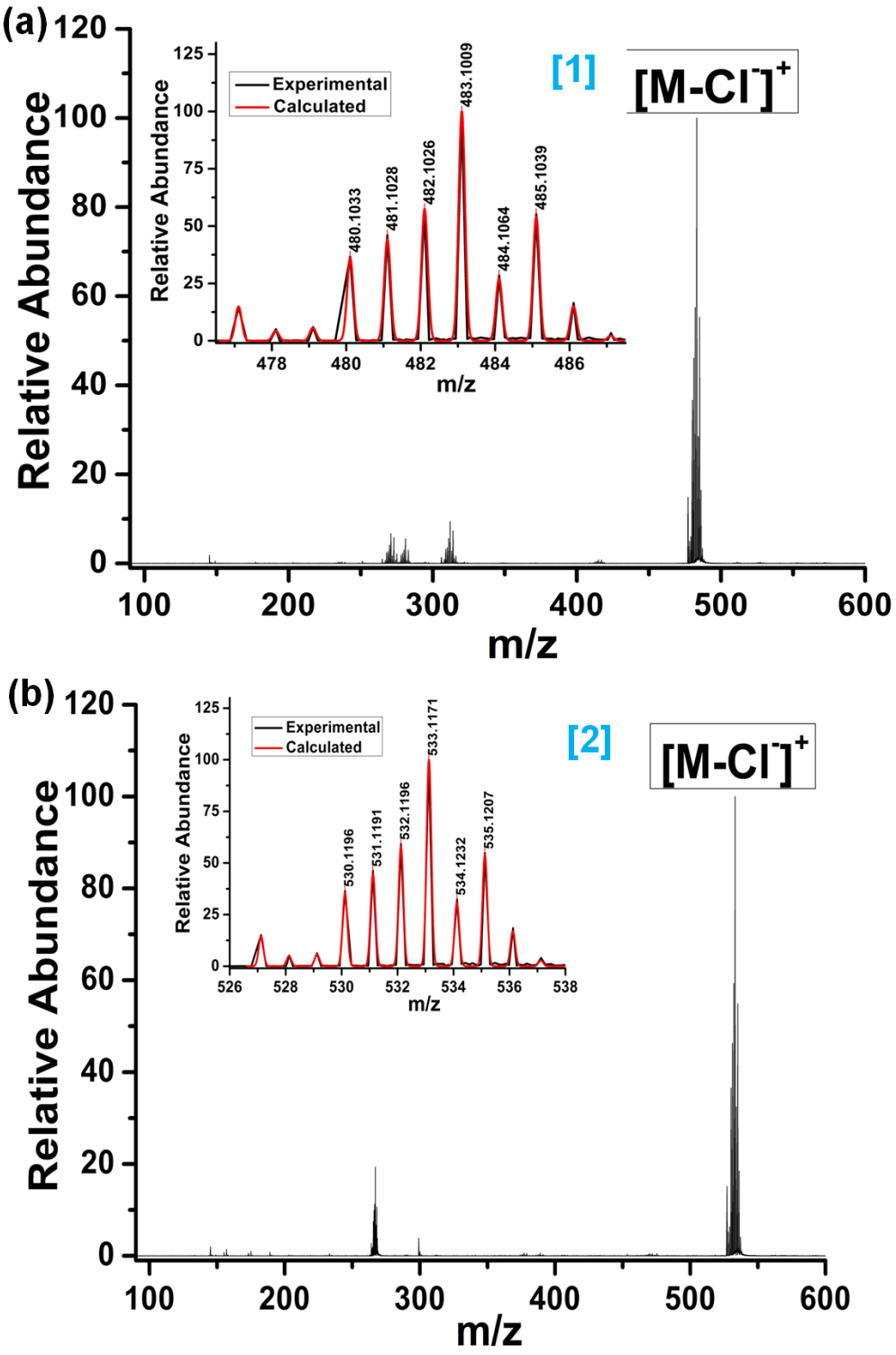

Figure S1. The positive ion mode ESI-MS analysis of the complexes (a) **1** showed $[M\text{-}Cl]^+$ and (b) **2** showed $[M\text{-}Cl]^+$ molecular ion peaks corresponding to the molecular mass M. Inset: The overlay of the theoretical and experimental isotopic distribution patterns of the molecular ions.

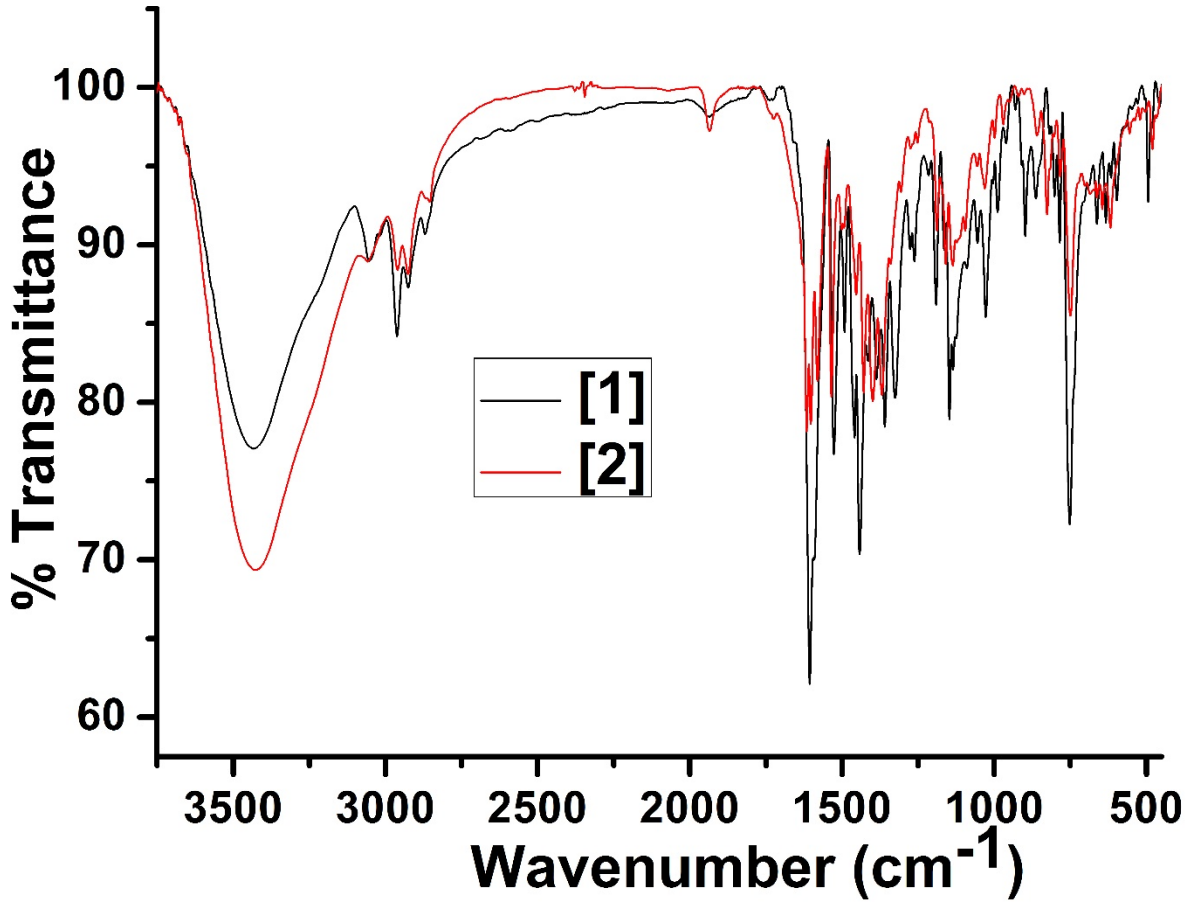

Figure S2. An overlay of the solid-state FTIR spectra of complexes **1** and **2** in KBr pellets.

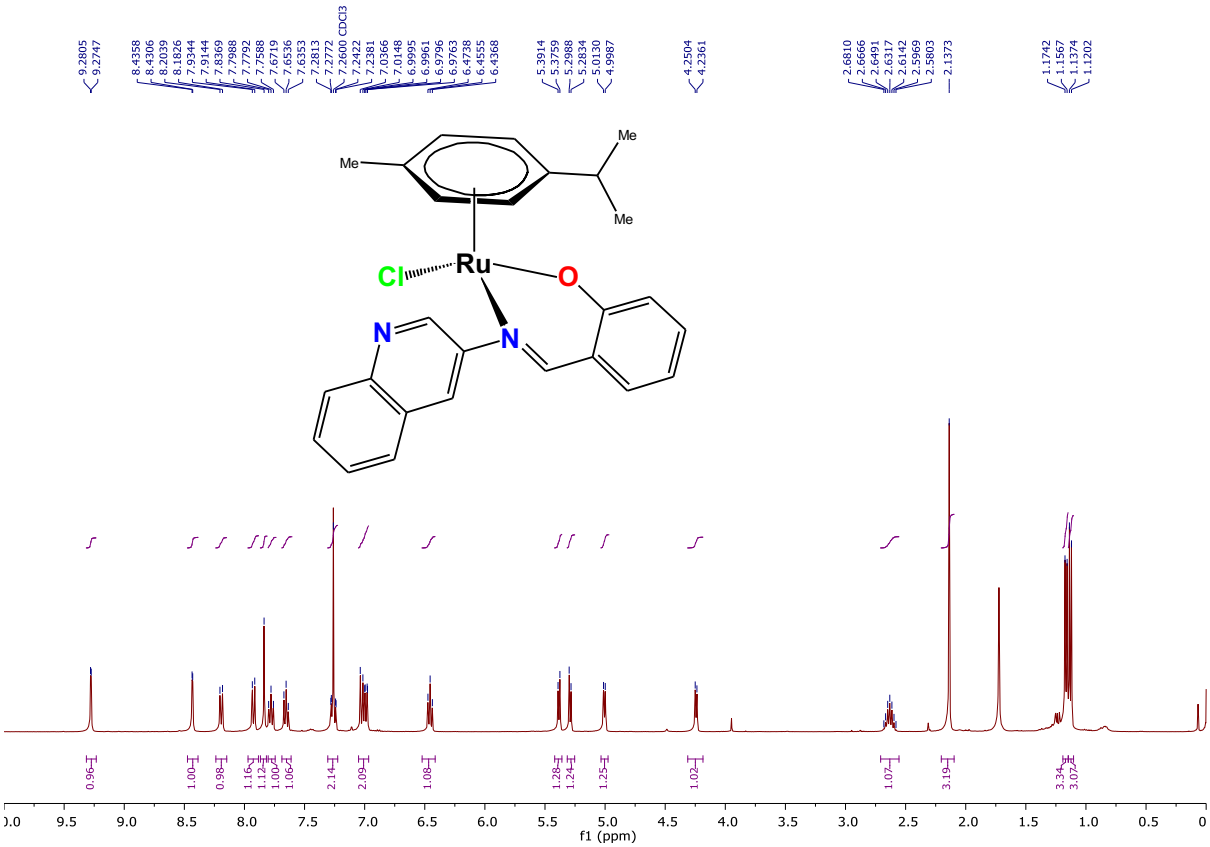

Figure S3. ^{1}H-NMR spectra of complex [Ru(η^6-*p*-cymene)(L1)Cl] (**1**) in $CDCl_3$ (referenced with $CDCl_3$ signal at 7.26 ppm) at 298 K.

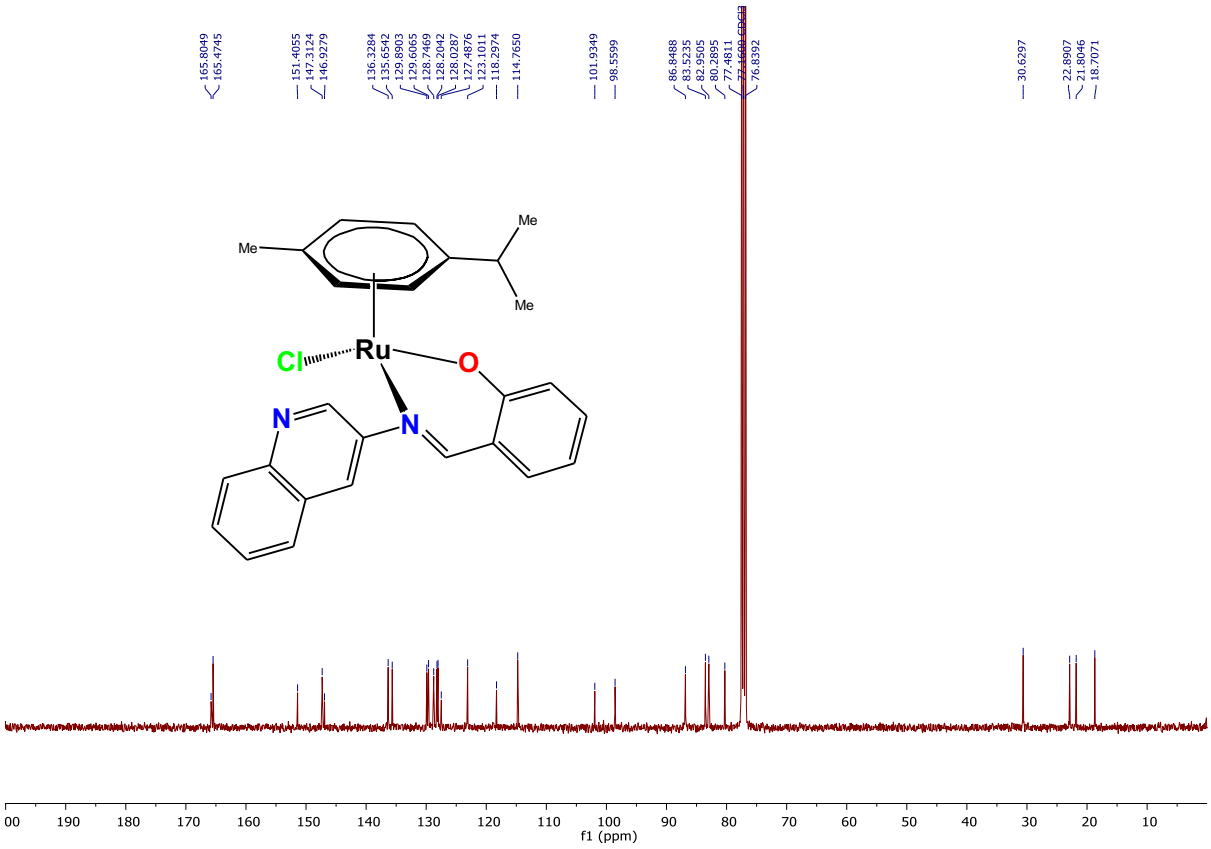

Figure S4. ^{13}C NMR spectra of [Ru(η^6-*p*-cymene)(L1)Cl] (**1**) in $CDCl_3$ at 298 K.

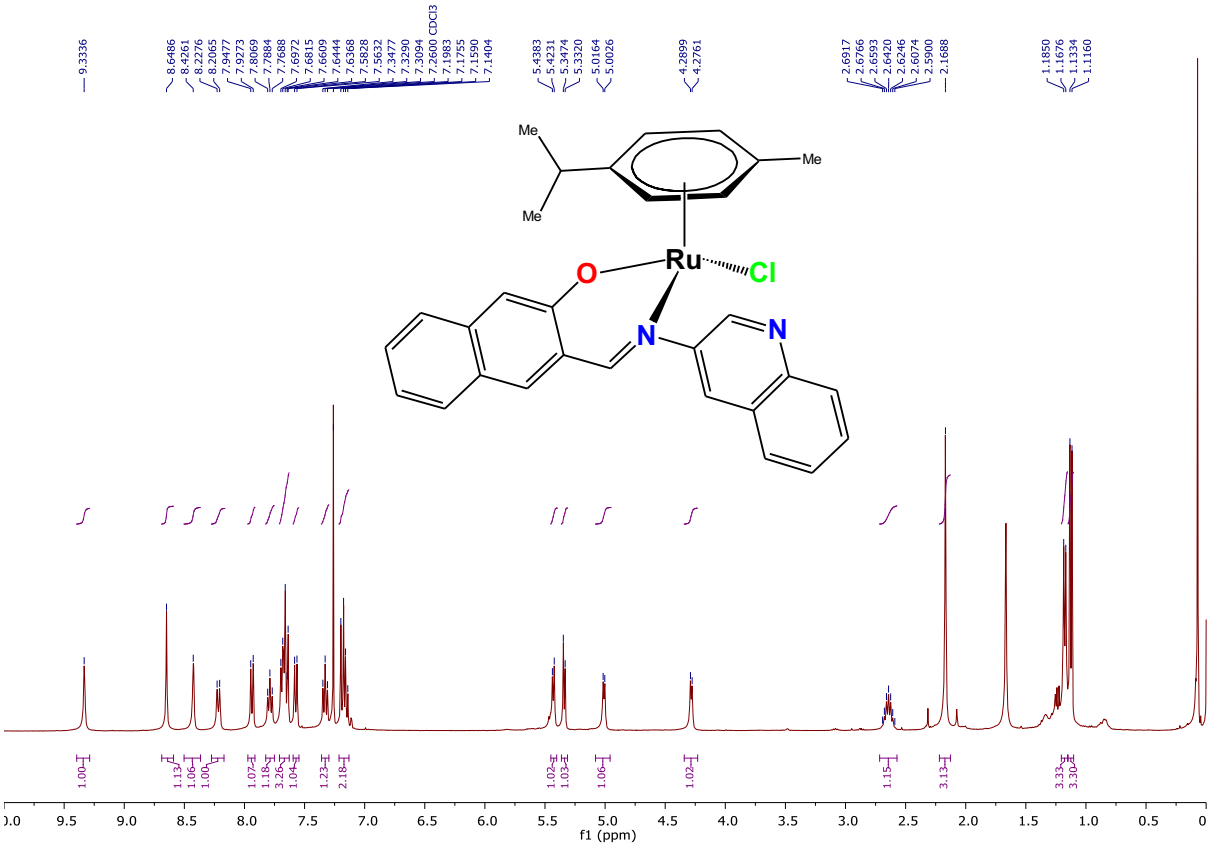

Figure S5. ^{1}H NMR spectra of complex [Ru(η^6-*p*-cymene)(L2)Cl] (**2**) in $CDCl_3$ (referenced with $CDCl_3$ signal at 7.26 ppm) at 298 K.

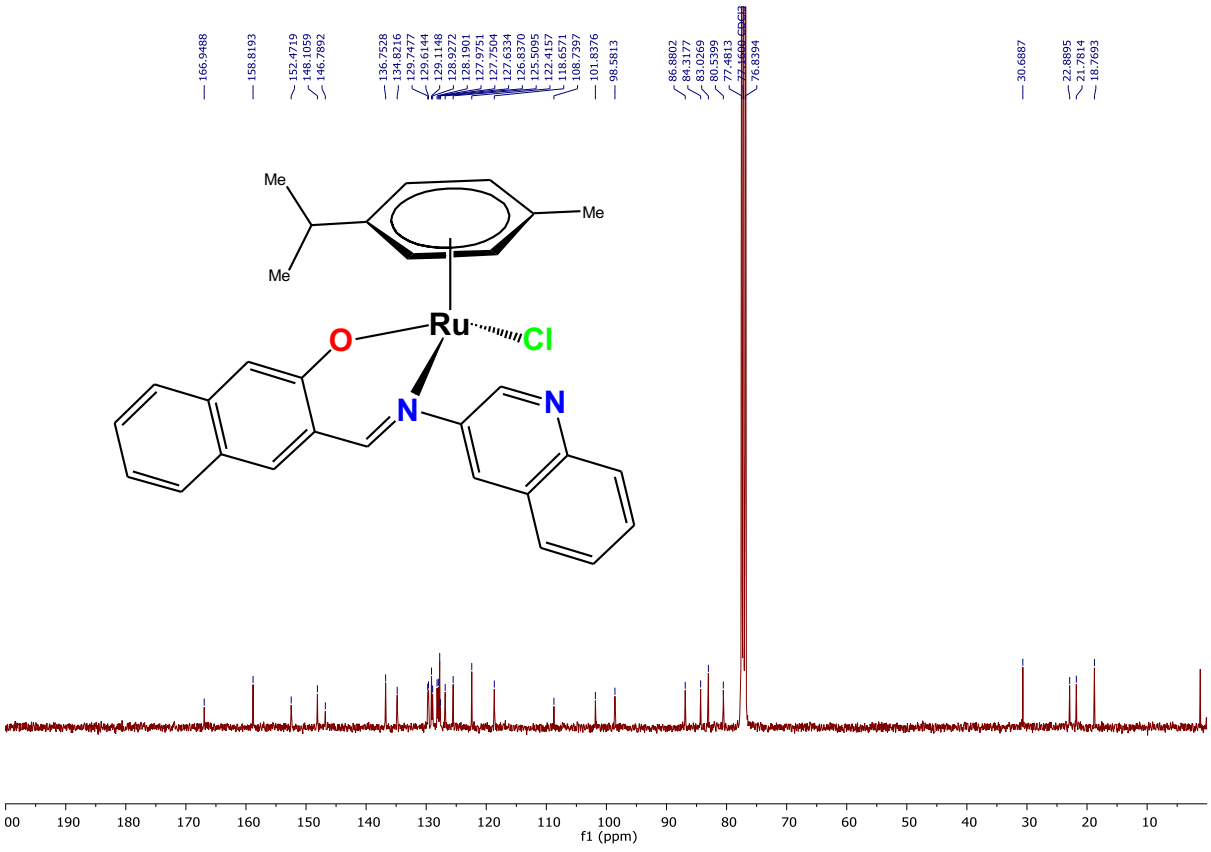

Figure S6. ^{13}C NMR spectra of [Ru(η^6-*p*-cymene)(L2)Cl] (**2**) in $CDCl_3$ at 298 K.

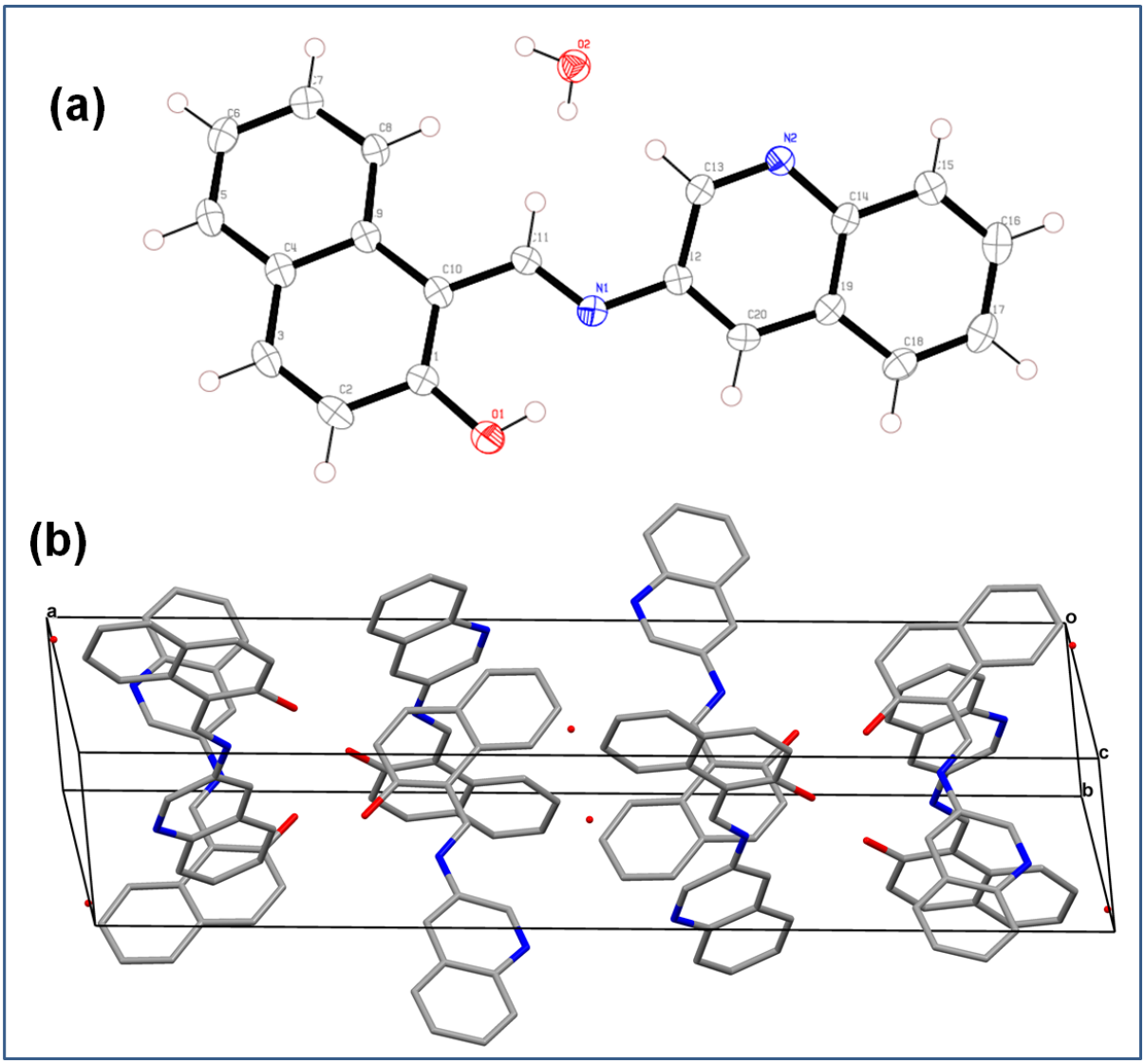

Figure S7. (a) An ORTEP view of the ligand L2•H_2O with the atom numbering scheme. (b) Unit cell of L•H_2O showing 8 molecules. The hydrogen atoms were removed for clarity.

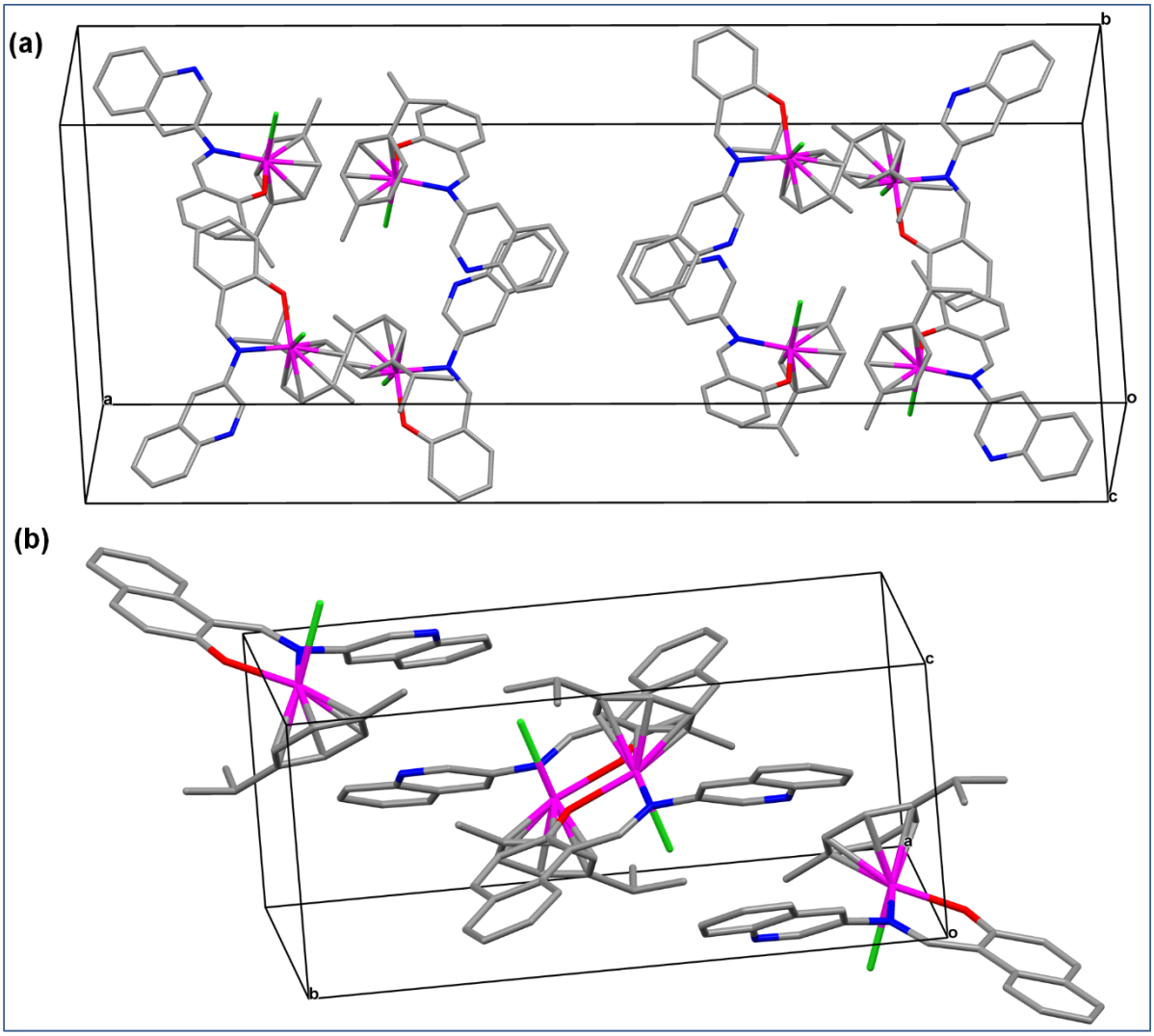

Figure S8. Unit cell of complexes **1** and **2** showing 8 and 4 molecules in respective unit cells. The hydrogen atoms were removed for clarity in the presentation.

Table S1. Selected crystallographic data and structure refinement parameters for the L2 and complexes **1** and **2**.

Parameters	L2	[Ru(η^6-*p*-cymene)(L1)Cl] (**1**)	[Ru(η^6-*p*-cymene)(L2)Cl] (**2**)
Empirical formula	$C_{40}H_{30}N_4O_3$	$C_{26}H_{25}ClN_2ORu$	$C_{30}H_{27}ClN_2ORu$
M_r	614.68	518.00	568.06
crystal system	Monoclinic	Monoclinic	Monoclinic
space group	*C*2/*c*	*C*2/*c*	$P2_1/c$
a (Å)	32.1158(18)	39.725(2)	20.1972(12)
b(Å)	4.7986(3)	16.7767(9)	17.0661(9)
c (Å)	22.4568(14)	7.7208(4)	7.6153(4)
α (deg)	90	90	90
β (deg)	122.361(3)	90.621(2)	99.273(2)
γ (deg)	90	90	90
Volume (Å^3)	2923.3(3)	5145.2(5)	2590.6(2)
Z	4	8	4
D_x (Mg m^{-3})	1.397	1.337	1.456
μ (mm^{-1})	0.090	0.731	0.734
F(000)	1288.0	2112.0	1160.0
T(K)	273.15	273.15	273.15
2θ range for data collection(deg)	5.188 to 50.098	5.272 to 56.728	4.774 to 56.726
Limiting indices	-38 ≤ h ≤ 38, -5 ≤ k ≤ 5, -26 ≤ l ≤ 26	-53 ≤ h ≤ 48, -22 ≤ k ≤ 22, -10 ≤ l ≤ 10	-26 ≤ h ≤ 26, -22 ≤ k ≤ 22, -10 ≤ l ≤ 10
Reflections collected	16548	25595	25590
unique reflections	2593	6427	6456
R(int)	0.0628	0.0916	0.0804
T_{max} / T_{min}	0.746/0.631	0.896/0.864	0.746/0.655
Data/restraints/parameters	2593/0/214	6427/0/283	6456/0/319
GOF on F^2	1.031	1.028	1.013
R_1[a] and wR_2[b] [$I>2\sigma(I)$]	R1 = 0.0452, wR2 = 0.0964	R1 = 0.0597, wR2 = 0.1223	R1 = 0.0536, wR2 = 0.1025
R_1 and wR_2 (all data)	R1 = 0.0792, wR2 = 0.1092	R1 = 0.1057, wR2 = 0.1369	R1 = 0.0932, wR2 = 0.1136
Largest diff. peak/ hole (e.A^{-3})	0.18/-0.27	1.39/-0.64	1.10/-0.54
CCDC deposition serial number	2006009	2006007	2006008

[a]$R_1 = \Sigma||F_o|-|F_c||/\Sigma|F_o|$; [b]$wR_2 = \{\Sigma[w(F_o^2-F_c^2)^2]/\Sigma[w(F_o^2)^2]\}^{1/2}$. Goodness-of-fit (GOF) $= \{\Sigma[w(F_o^2-F_c^2)^2/(n-p)]\}^{1/2}$, where n = number of data and p = number of parameters refined

Table S2 Selected bond length and bond angle parameter for the complexes **1** and **2**.

Bond lengths (Å) (**1**)		Bond lengths (Å) (**2**)	
Ru1-Cl1	2.4285(10)	Ru1-Cl1	2.4243(9)
Ru1-O1	2.078(3)	Ru1-O1	2.059(2)
Ru1-N1	2.097(4)	Ru1-N1	2.096(3)
Ru1-C20	2.185(4)	Ru1-C27	2.194(4)
Ru1-C18	2.210(4)	Ru1-C26	2.171(3)
Ru1-C22	2.175(4)	Ru1-C22	2.205(3)
Ru1-C23	2.184(4)	Ru1-C23	2.193(3)
Ru1-C19	2.192(4)	Ru1-C25	2.197(3)
Ru1-C21	2.209(4)	Ru1-C24	2.172(3)
Bond Angles (deg)		**Bond Angles (deg)**	
O1-Ru1-Cl1	85.55(8)	O1-Ru1-Cl1	84.86(7)
O1-Ru1-N1	87.92(13)	O1-Ru1-N1	86.60(10)
O1-Ru1-C20	128.23(14)	O1-Ru1-C27	106.74(12)
O1-Ru1-C18	140.77(14)	O1-Ru1-C26	86.56(11)
O1-Ru1-C22	85.73(14)	O1-Ru1-C22	142.99(12)
O1-Ru1-C23	104.78(14)	O1-Ru1-C23	163.05(11)
O1-Ru1-C19	163.59(14)	O1-Ru1-C25	94.67(11)
O1-Ru1-C21	95.25(14)	O1-Ru1-C24	127.05(12)
N1-Ru1-Cl1	84.93(10)	N1-Ru1-Cl1	85.10(8)
N1-Ru1-C20	91.32(15)	N1-Ru1-C27	166.65(12)
N1-Ru1-C18	130.06(15)	N1-Ru1-C26	147.81(12)
N1-Ru1-C22	146.05(15)	N1-Ru1-C22	129.14(12)
N1-Ru1-C23	167.26(15)	N1-Ru1-C23	99.91(12)
N1-Ru1-C19	100.25(15)	N1-Ru1-C25	111.56(12)
N1-Ru1-C21	110.02(15)	N1-Ru1-C24	92.02(12)
C20-Ru1-Cl1	145.92(12)	C27-Ru1-Cl1	95.39(10)

C20-Ru1-C18	68.49(16)	C27-Ru1-C22	37.69(13)
C20-Ru1-C19	38.27(16)	C27-Ru1-C25	68.71(14)
C20-Ru1-C21	37.60(15)	C26-Ru1-Cl1	125.48(10)
C18-Ru1-Cl1	88.26(11)	C26-Ru1-C27	37.50(13)
C22-Ru1-Cl1	127.62(11)	C26-Ru1-C22	67.91(13)
C22-Ru1-C20	67.34(16)	C26-Ru1-C23	79.59(13)
C22-Ru1-C18	67.90(16)	C26-Ru1-C25	37.99(13)
C22-Ru1-C23	37.27(15)	C26-Ru1-C24	67.70(13)
C22-Ru1-C19	79.54(16)	C22-Ru1-Cl1	88.71(9)
C22-Ru1-C21	37.88(15)	C23-Ru1-Cl1	111.14(9)
C23-Ru1-Cl1	96.89(11)	C23-Ru1-C27	67.42(13)
C23-Ru1-C20	80.08(16)	C23-Ru1-C22	37.48(13)
C23-Ru1-C18	37.78(15)	C23-Ru1-C25	68.39(13)
C23-Ru1-C19	67.21(16)	C25-Ru1-Cl1	163.30(10)
C23-Ru1-C21	68.42(16)	C25-Ru1-C22	81.62(13)
C19-Ru1-Cl1	109.18(11)	C24-Ru1-Cl1	147.81(10)
C19-Ru1-C18	37.23(15)	C24-Ru1-C27	80.44(13)
C19-Ru1-C21	68.62(15)	C24-Ru1-C22	68.43(13)
C21-Ru1-Cl1	165.04(12)	C24-Ru1-C23	37.82(13)
C21-Ru1-C18	81.66(15)	C24-Ru1-C25	37.85(13)

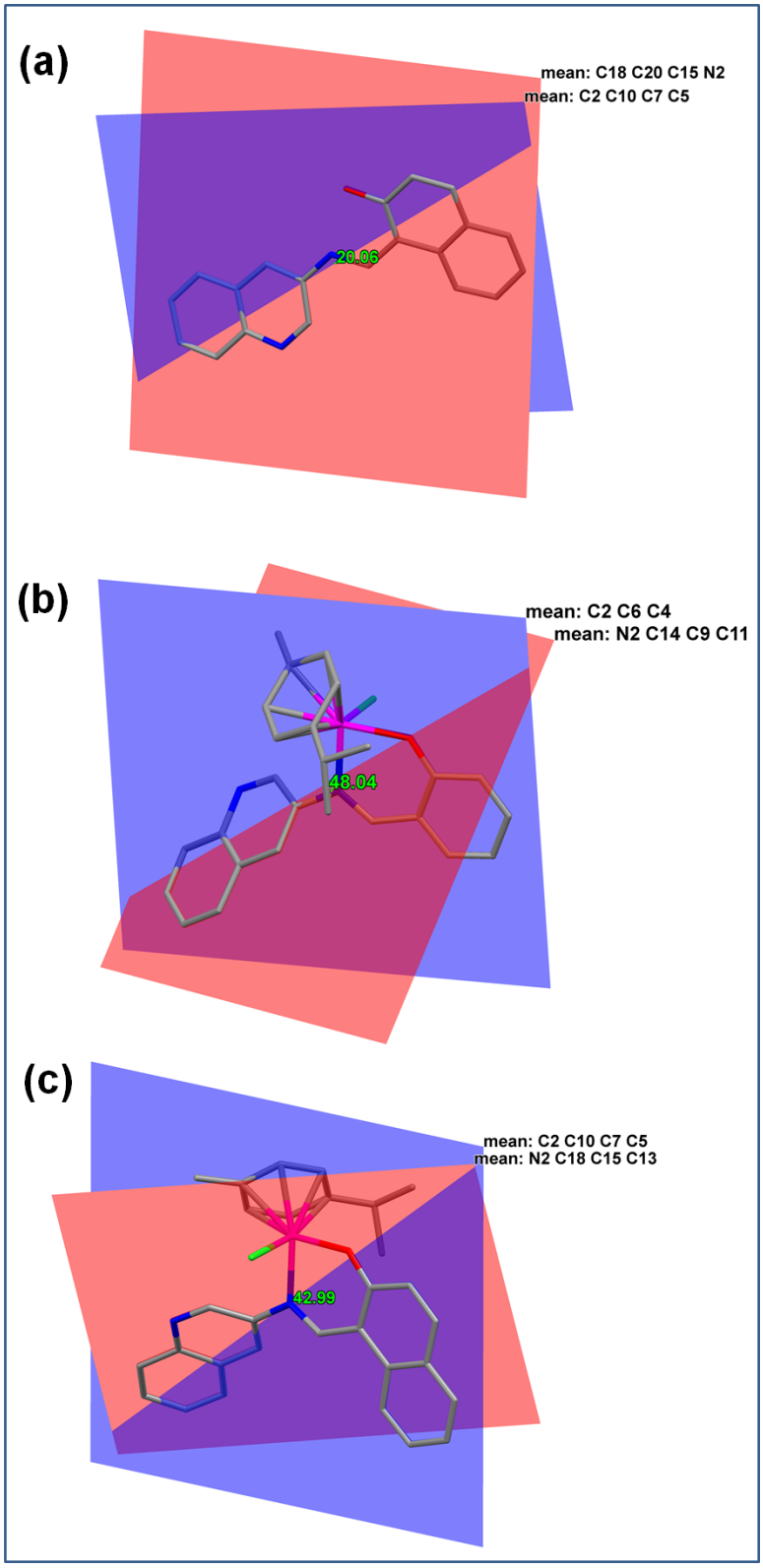

Figure S9. Representation of the dihedral angles (a) between the planes containing [C18 C20 C15 N2] and [C2 C10 C7 C5] atoms of L2 (b) between the planes carrying [N2 C14 C9 C11] and [C2 C6 C4] atoms of complex **1**, and (c) between the planes containing [N2 C18 C15 C13] and [C2 C10 C7 C5] atoms of complex **2**.

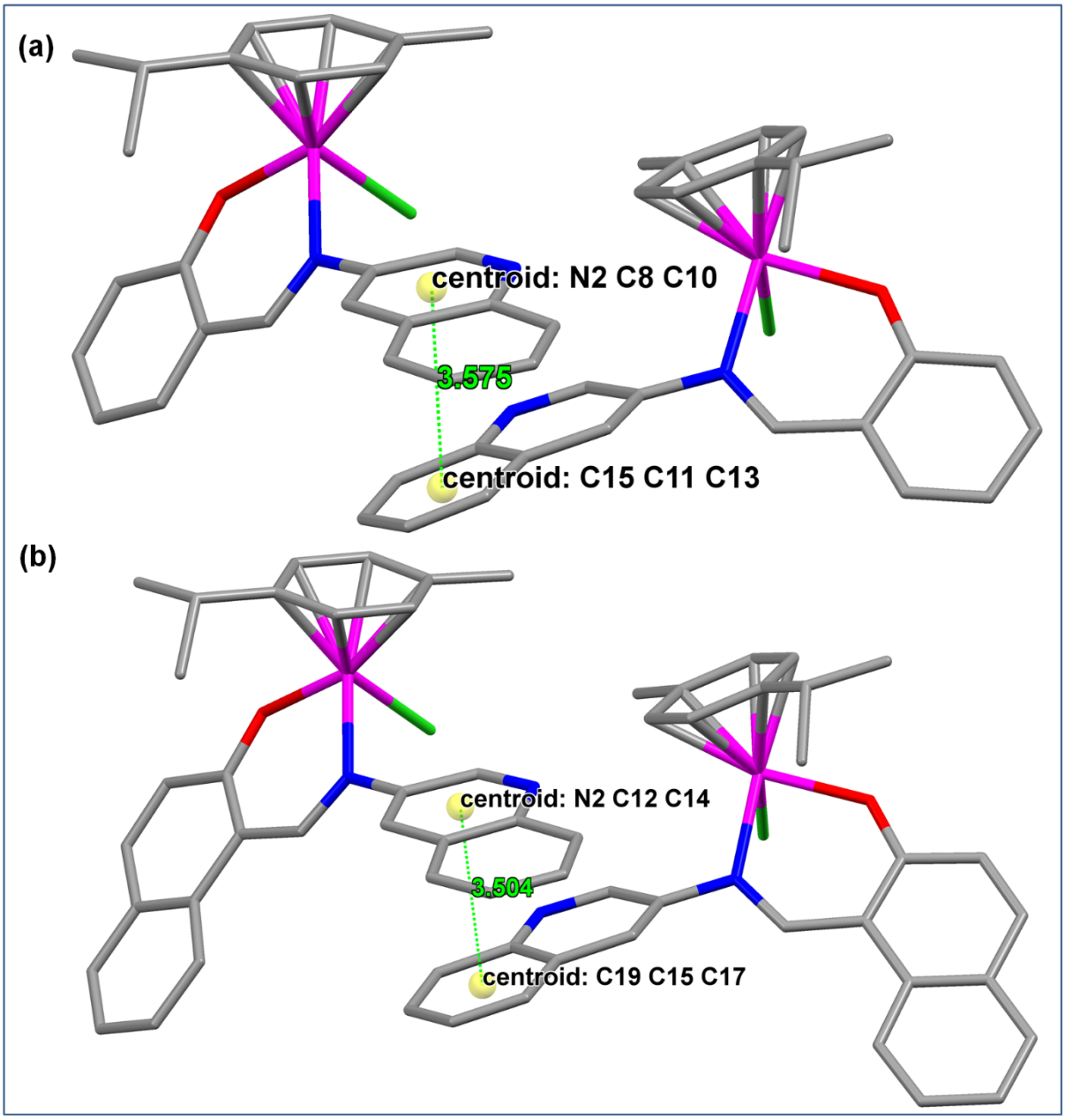

Figure S10. Intermolecular π–π stacking interaction between quinoline rings of the complexes (a) **1** and (b) **2**.

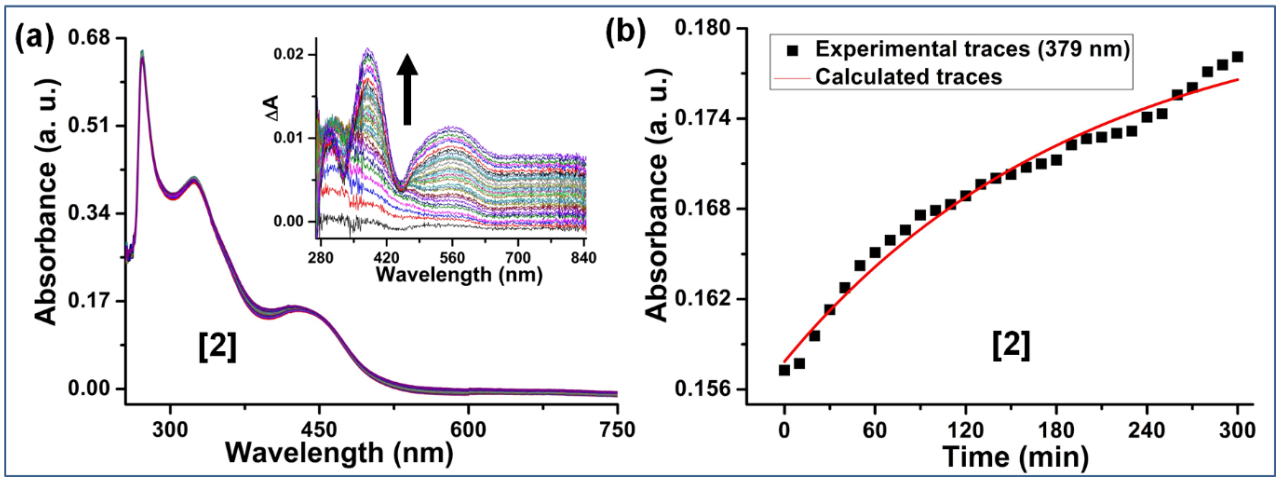

Figure S11. (a) The changes in absorption spectral profile for the complex **2** (39 μM) in 5 mM tris HCl-NaCl buffer (pH = 7.2)-DMF mixture (1: 1) at 298 K. Inset: Evolution of UV-visible difference spectra upon aquation of complex **2**. (b) Absorption traces at 379 nm and mono-exponential fit upon hydrolysis for complex **2**.

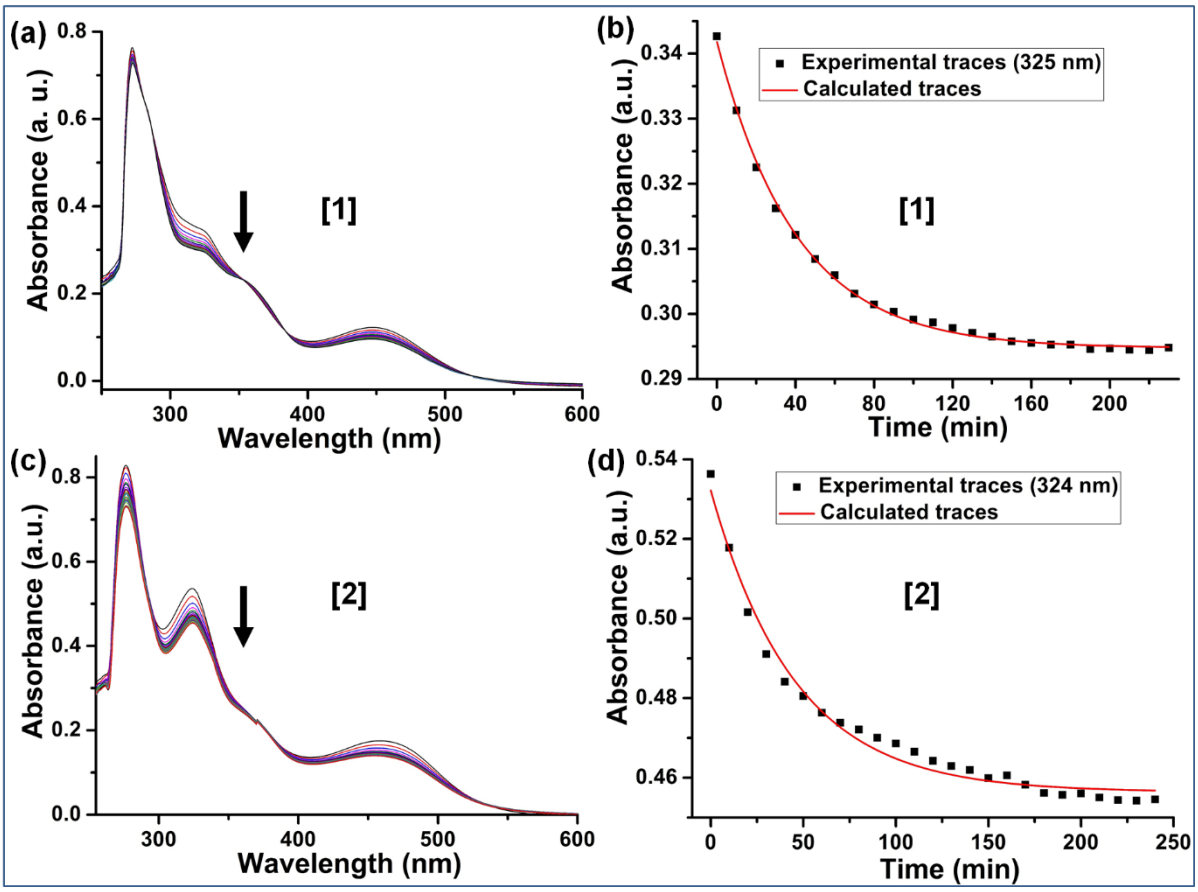

Figure S12. The changes in the absorption spectral profile of the complexes (a) **1** (39 μM) and (c) **2** (39 μM) in DMF. (b) The changes in absorbance at 325 nm (**1**) as a function of time with their mono-exponential fit. (d) The changes in absorbance at 324 nm (**2**) as a function of time with their mono-exponential fit.

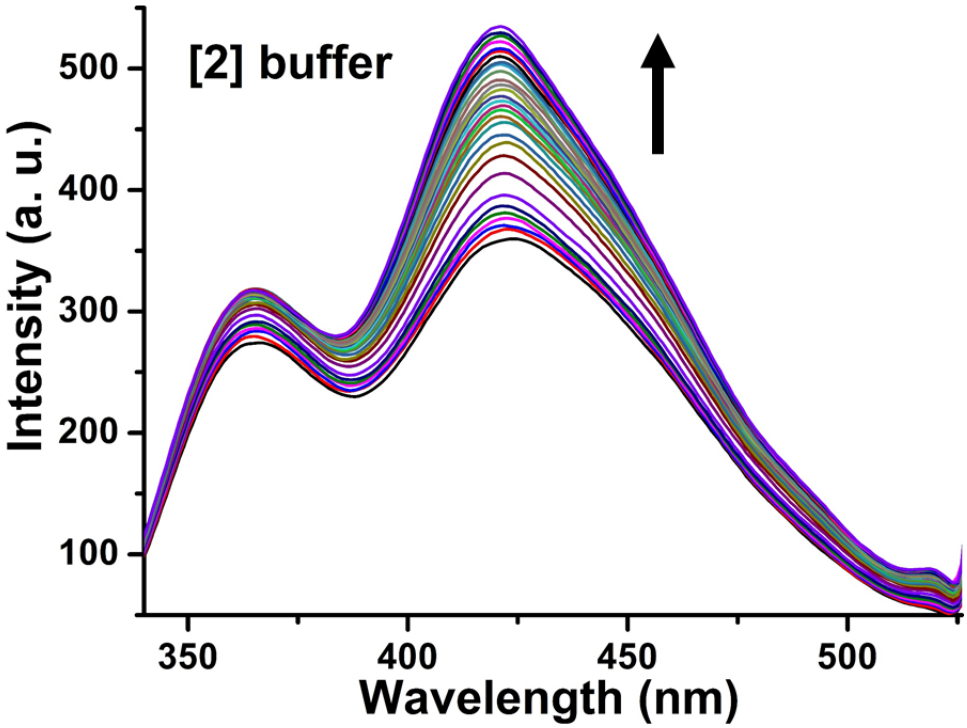

Figure S13. The time-dependent changes in fluorescence spectral profile for the complex **2** (10 μM) in 5 mM Tris HCl/NaCl buffer (pH = 7.2)-DMF mixture (200:1).

Table S3. The photochemical results of complexes **1**and **2** upon photo-irradiation of UV-A light (λ_{exc} = 365 nm and power = 6 W).

Complex	[a]K (s^{-1})	[b]$t_{1/2}$ (min)
1	(7.96±0.46) × 10^{-4}	14.51
2	(6.79±0.59) × 10^{-4}	17.01

[a]First-order rate constant of photochemical changes determined from monoexponential curve fitting with R^2 = 0.99 for both the complexes **1** and **2** . [b]Half-lifetime for the photo-induced product formation.

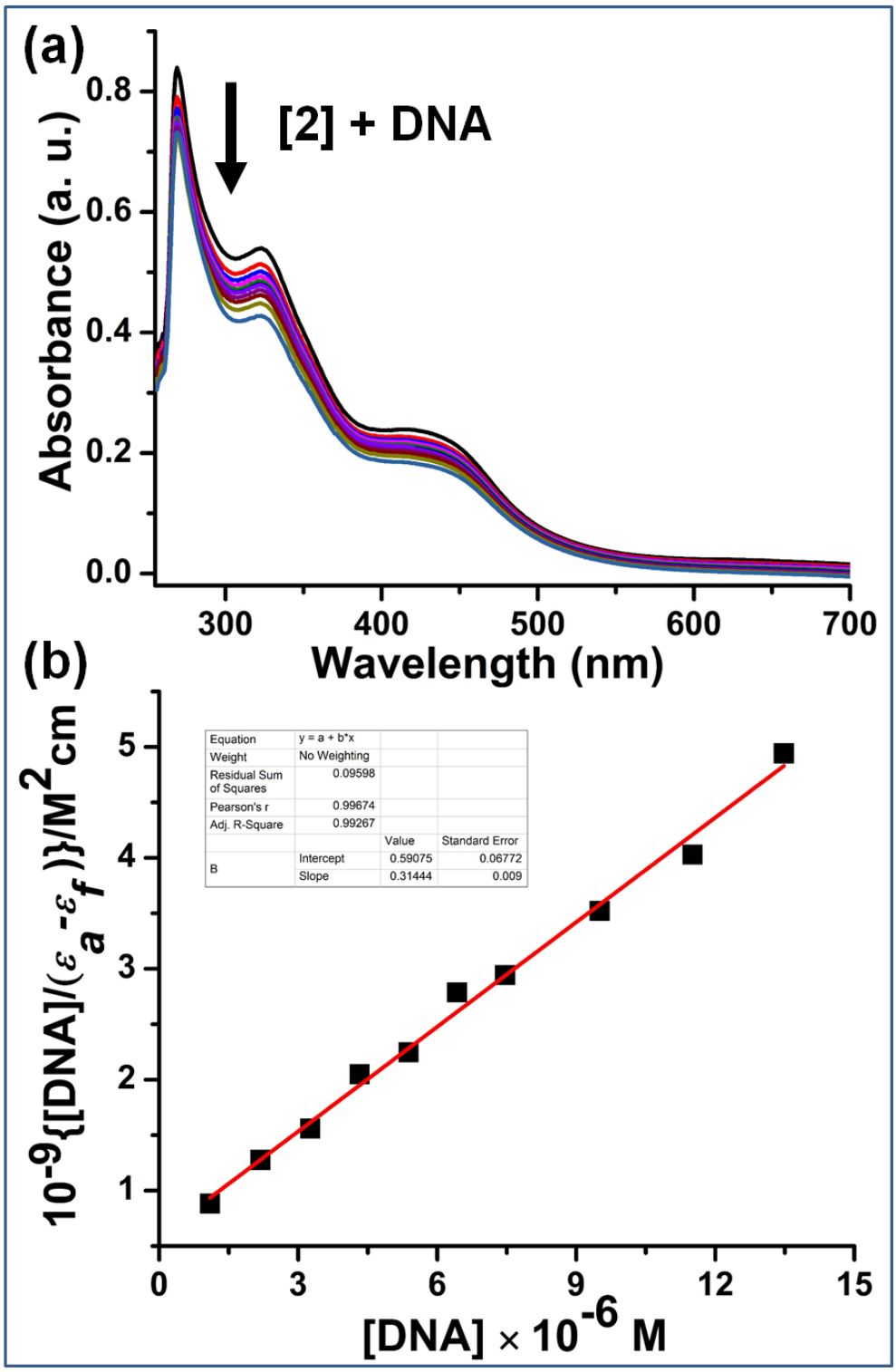

Figure S14. The binding propensity of the complexes with CT-DNA. (a) The continuous decrease of absorbance of complex **2** (39 μM) upon gradual addition of CT-DNA (0–15 μM) in 5 mM Tris HCl-NaCl buffer (pH = 7.2)-DMF mixture (50: 1). (b) Determination of binding constant (K_b) of complex **2** with CT-DNA from the slope to intercept ratio of a linear fitted plot of [DNA] vs DNA/ε_a-ε_f from equation (3).

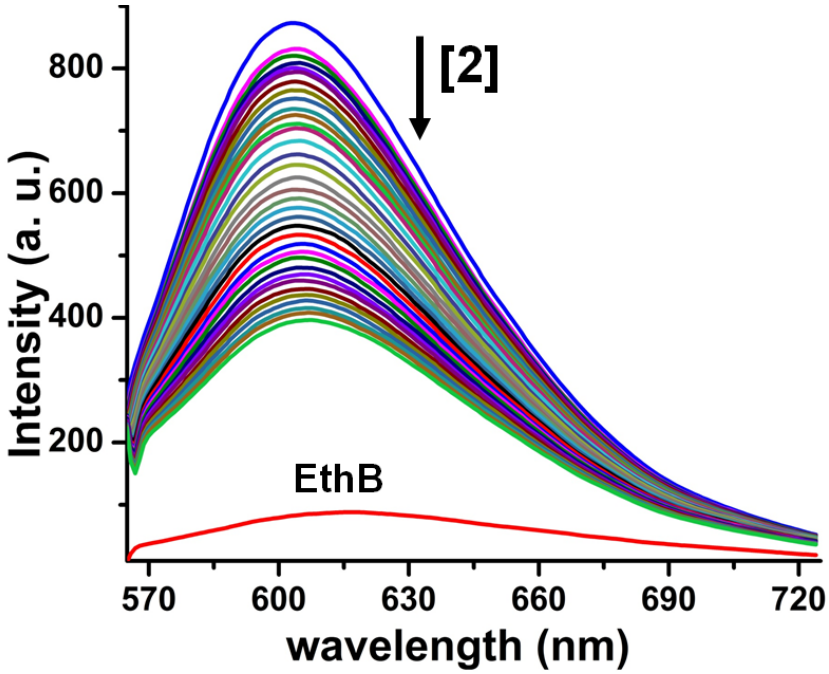

Figure S15. The decrease of emission intensity of EthB (12.5 μM) bound CT-DNA (10 μM) upon addition of complex **2** (0–236 μM), λ_{ex} = 546 nm, Ex and Em slit width = 10 nm.

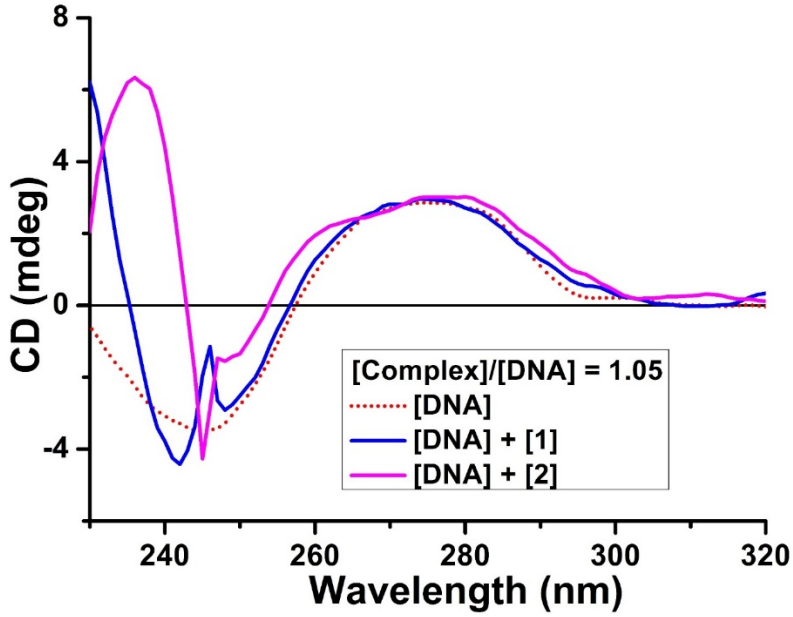

Figure S16. An overlay of circular dichroism spectra of CT-DNA (225 μM) and induced CD signals from the complexes **1** and **2**.

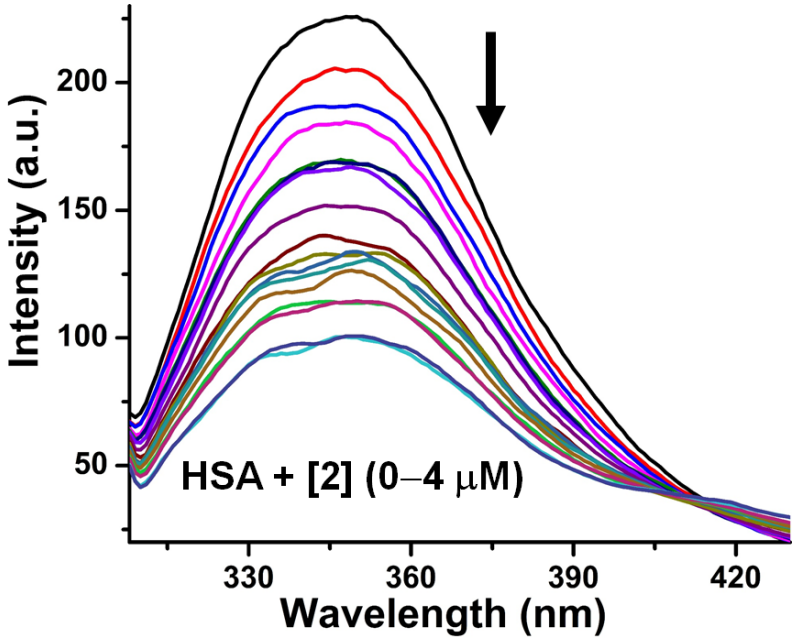

Figure S17. The result of the binding of the complexes with protein HSA. (a) The quenching of emission intensity of HSA (2.4 μM) in absence and in presence of increasing concentration complex **2** (0–4 μM) in 0.8% DMF-5mM Tris-HCl/NaCl buffer (pH 7.2) mixture, λ_{exc} = 295 nm, λ_{em} = 350 nm, slit 10/5 nm.

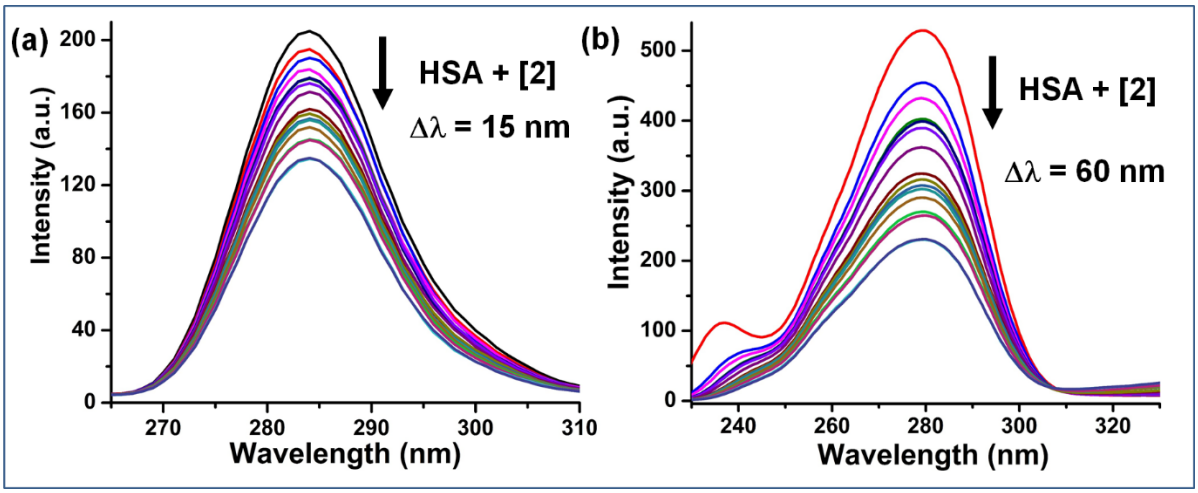

Figure S18. The synchronous fluorescence measurement of HSA (2.4 μM) upon addition of complex **2** (0–4 μM) in 0.8% DMF-5mM Tris-HCl/NaCl buffer (pH 7.2) mixture at 298 K. (a) Spectral traces of the HSA upon titration with complex **2** for $\Delta\lambda$ = 15 nm. (b) Spectral traces of the HSA upon titration with complex **2** for $\Delta\lambda$ = 60 nm, Slit width for exc/em = 10/5 nm.